Materials Advances

ROYAL SOCIETY OF CHEMISTRY

PAPER

View Article Online
View Journal | View Issue

Cite this: *Mater. Adv.*, 2026, 7, 2481

UV-induced near-white visible emission in dinuclear Tb(III) complexes: a photophysical, theoretical and computational study on fluxidentate ligand bridging and coordination geometry

Vandana Aggarwal,[a] Devender Singh,*[a] Vandna Nishal,[a] Anuj Dalal,[b] Sumit Kumar,[c] Rajender Singh Malik,[c] Parvin Kumar,[d] Jayant Sindhu[e] and Varun Kumar[f]

In this work, three Tb(III) complexes, TbA, TbM and TbD, were synthesized using 4,4,4-trifluoro-1-(2-thienyl)-1,3-butanedione (TTBD) and pyrazine (pyz) as antenna moieties. Structural characterizations (elemental (CHN), infrared and NMR) confirmed that TbA and TbM are mononuclear and share an identical structural framework, while TbD forms a dinuclear species where pyrazine serves as a bridging ligand. Photoluminescent (PL) features of the complexes were studied through electronic absorption, PL and lifetime analyses. All three complexes emit the characteristic emissive peaks of Tb(III) ions along with a broad ligand-centered band due to the sensitizer energy difference. Upon incorporation of chromophores, the emission color shifts dramatically towards near-white, showcasing tunable optical behavior. The Judd–Ofelt analysis supported these photophysical observations theoretically. Detailed decay studies provided radiative lifetime data and insights into the qualitative energy transfer efficiency from the ligand to the metal. Bandgap analysis using Tauc's method, supported by DFT calculations revealed semiconducting behavior with a value of ~3.2 eV. These outcomes highlight the possibility of these complexes for use in photonic and optoelectronic applications, highlighting how pyrazine incorporation enables fine-tuning of Tb(III) luminescence to achieve near-white emission.

Received 6th October 2025,
Accepted 15th January 2026

DOI: 10.1039/d5ma01145k

rsc.li/materials-advances

1. Introduction

Lanthanide complexes are of particular interest in several areas, including single-molecule magnets,[1] electroluminescent devices,[2] laser systems,[3] sensors[4] and optical communications.[5] However, despite their wide range of potential applications, the fluorescence intensities and deactivation times of Ln(III) ions are often limited as their f–f electronic transitions are inherently forbidden in nature.[6] To overcome this limitation, a wide range of organic ligands including aromatic 1,3-diketones have been incorporated into lanthanide complexes, although their efficiency varies depending on the system.[7] These organic ligands possess excellent light absorption capabilities and can transfer energy to the Ln(III) ions through a phenomenon recognized as the antenna effect, thus enhancing their luminescent properties.[8] From this perspective, heteroaryl β-diketones (TTBD) have been explored for their ability to form stable complexes with lanthanide ions. These ligands bind to lanthanide ions *via* bidentate chelation, forming six-membered rings that further stabilize the complex and enhance its properties. Typically, the energy gaps between excited ligand states and excited 4f states are $<5000\ cm^{-1}$, with the ligand having a higher energy to facilitate efficient energy transfer.[9] Current studies have shown that bipyridine moieties like 4,4′-bipyridine/bis-pyridylethane are highly effective antennas for Ln(III) ions.[10] For example, sensitization was observed outside the optimal energy gap for Nd(III) or Er(III) with bis-pyridylethylene when thiazole was used as a neutral ligand. Interestingly, such ligands could efficiently sensitize Ln(III) ions

[a] *Department of Chemistry, Maharshi Dayanand University, Rohtak-124001, Haryana, India. E-mail: devjakhar@gmail.com*
[b] *Department of Chemistry, School of Sciences, Noida International University, Greater Noida, Uttar Pradesh, 203201, India*
[c] *Department of Chemistry, DCR University of Science & Technology, Murthal - 131039, Haryana, India*
[d] *Department of Chemistry, Kurukshetra University, Kurukshetra - 136119, Haryana, India*
[e] *Department of Chemistry, COBS&H, CCS Haryana Agricultural University, Hisar-125004, Haryana, India*
[f] *Department of Computer Science and Engineering, UIET, Maharshi Dayanand University, Rohtak-124001, Haryana, India*

either in the visible or near-infrared (NIR) region. As a result, we expanded our research for efficient sensitizers to include diazines, specifically pyrazine (pyz). By combining it with 1,3-diketonate lanthanide chelates, different complexes were synthesized. These complexes demonstrated effective sensitization for Tb(III) ions in the visible range as presented here.

Pyrazine (pyz), with its rigid heteroaromatic conjugated π-system, has emerged as a particularly effective ligand for this purpose. It functions as a monodentate as well as a bidentate (*via* bridging) chromophore in metal complexes, coordinating *via* its –N in the ring. This not only increases the chemical and thermal stability of the resulting complexes but also contributes to enhanced luminescence by matching the triplet energy (T_1) level of pyz with the excited state energy level of Tb(III), further boosting the fluorescence intensity. In the field of OLEDs (organic light-emitting diodes), lanthanide tris(β-diketone) complexes are emerging as promising materials.[11–13] These complexes exhibit line-like emission due to 4f–4f transitions from the emitting state of Ln(III) ions. Excitation of the Ln(III) ions occurs through intramolecular energy transfer from T_1 of the ligands, as well as from singlet to triplet (T_1) state relaxation *via* ISC (intersystem crossing). Luminescent devices based on Eu(III), Tb(III) and Dy(III) complexes are highly significant, as they produce sharp, line-like emission bands in the red (R), green (G) and white/yellow (Y) regions, respectively.[14] For improving the performance of OLEDs, scientists have prepared a wide array of Ln(III) complexes by introducing specific changes, such as doping. Despite the progress, there is still an ongoing need for the development of improved electroluminescent materials containing Ln(III) ions for the fabrication of novel and more efficient devices.

This study introduces a combination of a neutral pyz ligand and an anionic 4,4,4-trifluoro-1-(2-thienyl)-1,3-butanedione ligand (TTBD) to synthesize three distinct terbium complexes. Here, two mononuclear eight-coordinated complexes, $[Tb(TTBD)_3(H_2O)_2]$ and $[Tb(TTBD)_3(pyz)_2]$, and a binuclear seven-coordinated complex $[Tb_2(TFPB)_6(pyz)]$ have been synthesized. The synthesis, structural characterization, luminescence and semiconducting behavior of these complexes have been discussed in detail, demonstrating how the choice of ligand and coordination environment can significantly influence the performance of the final complex in various applications. Although not among the most efficient antenna ligands, TTBD and pyz were chosen because their coordination with Tb(III) ions affords blue emission from the ligand itself. The resulting complementary emission can approach white light, thereby enabling the design of single-component white-light emitters, an aspect central to the novelty of this study. This ability of these Tb(III) complexes is of practical significance. Compared to multi-component emitting systems, single-component white-light emitters avoid issues such as phase separation, differential degradation and color instability arising from component migration or uneven energy transfer. This design strategy simplifies device fabrication and enhances reproducibility, while offering improved operational stability. Such features are particularly advantageous for solid-state lighting and display applications where consistent color output and device reliability are essential. In conclusion, the development and study of lanthanide coordination complexes, particularly those incorporating multidentate ligands like pyz and β-diketones, represents an exciting frontier in materials science and device engineering. The ability to control the electronic properties of these complexes opens up numerous possibilities for applications in fields such as optoelectronics, photonics[15] and biomedical diagnostics.[16] As research continues to evolve, the potential for lanthanide complexes in advanced technologies is vast, offering new solutions and innovations across a wide range of industries.

2. Materials and techniques

The synthesis process begins with commercially available solid starting materials, including the metal salt, terbium chloride ($TbCl_3{\cdot}6H_2O$), and coordinating ligands, 1,3-diketone (TTBD) and pyrazine (pyz), which are used directly. All of these were sourced from Sigma-Aldrich. Additionally, the ammonia solution (25%) and the solvents used, such as ethanol and hexane, were of analytical or spectroscopic grade (AG/SG). For the primary CHN analysis of the synthesized complexes, an elemental analyzer (PerkinElmer, model 2400) was used. The Fourier-transform infrared profiles were recorded in the 400–4000 cm^{-1} range on a PerkinElmer FTIR spectrophotometer (model 5700), with the samples converted into pellets using KBr as the standard reference. Proton magnetic resonance (PMR) profiles were obtained using a 400 MHz FT NMR Spectrometer in $CDCl_3$, with TMS as the reference (δ/chemical shift). Optical absorbance spectra of the samples in dichloromethane (DCM) in the UV-visible range (200–800 nm) were recorded using a Shimadzu UV-Vis Spectrophotometer (model 2450). Optical excitation profiles were recorded by monitoring emission at 545 nm in the 200–600 nm wavelength range and photoluminescence (PL) emission spectra at the respective excitation wavelengths were measured in the solution phase ($c = 10^{-5}$ M) using DCM as the solvent on a Horiba Jobin-Yvon Fluorolog FL-3–11 Spectrophotometer with a 450 W Xe lamp. Decay lifetimes of the complexes were measured using an F-7000 FL Spectrophotometer, with excitation at 545 nm and a 20 ms scan rate. Thermal decomposition patterns were acquired with a Hitachi STA-7300 Analyser in an inert N_2 environment at a heating rate of 10 °C min^{-1}. Computational studies were performed using Orca and Avogadro software. All spectroscopic analyses were performed at room temperature (RT), unless stated otherwise.

3. Synthesis

3.1. $[Tb(TTBD)_3(H_2O)_2]$

The procedure shown in Fig. 1 was followed to synthesize the binary Tb(III) complex with TTBD, *i.e.* $[Tb(TTBD)_3(H_2O)_2]$ (TbA).[17,18]

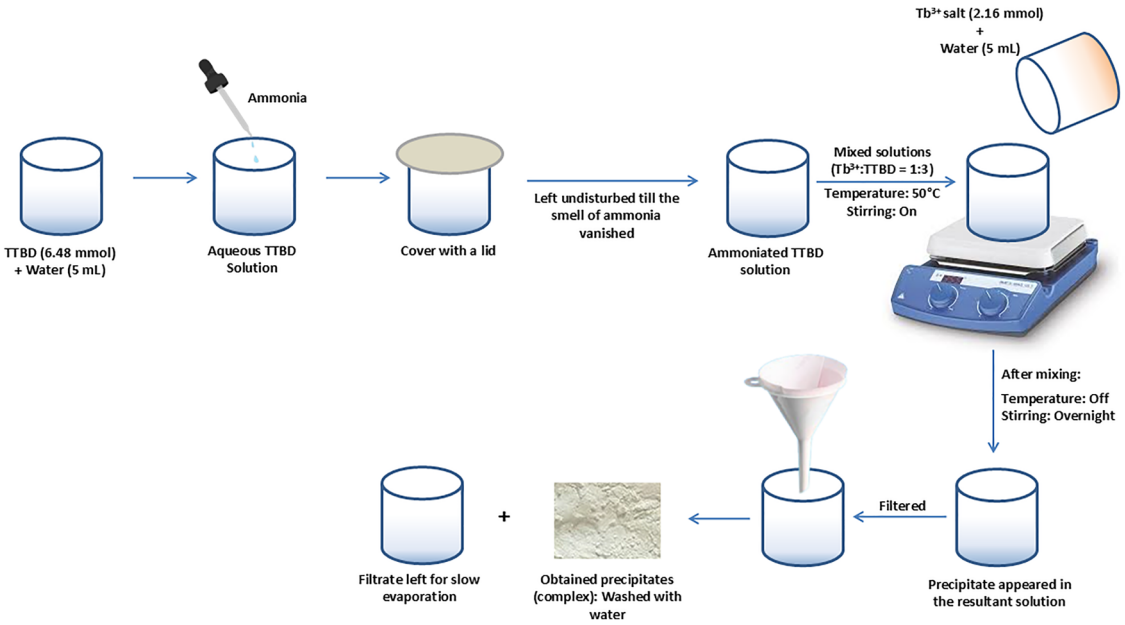

Fig. 1 Synthesis pathway for TbA.

3.2. $[Tb(TTBD)_3(pyz)_2]$

The procedure shown in Fig. 2 was followed to synthesize the ternary Tb(III) complex with TTBD and pyz, *i.e.* $[Tb(TTBD)_3(pyz)_2]$ (TbM).[19,20]

3.3. $[(Tb(TTBD)_3)_2\ pyz]$

The procedure shown in Fig. 3 was followed to synthesize the desired seven-coordinated binuclear complex $[Tb_2(TTBD)_6(pyz)]$. The prepared complexes were comprehensively characterized using several analytical and spectroscopic techniques.[21,22]

4. Results and discussion

4.1. CHN study

The TbA (mononuclear precursor) complex when coordinated with pyz forming TbD was obtained as a cream solid, while the complexes TbA and TbM appeared beige. Based on the elemental analysis, the empirical formulae were deduced and found to be in good agreement with theoretical values, with calculated minimal deviations validating the outcomes. Table 1 provides theoretical (T) and experimental (E) percentages of C, N and H contents for all the complexes, along with their respective formulae. The reaction yields (in percentage) for

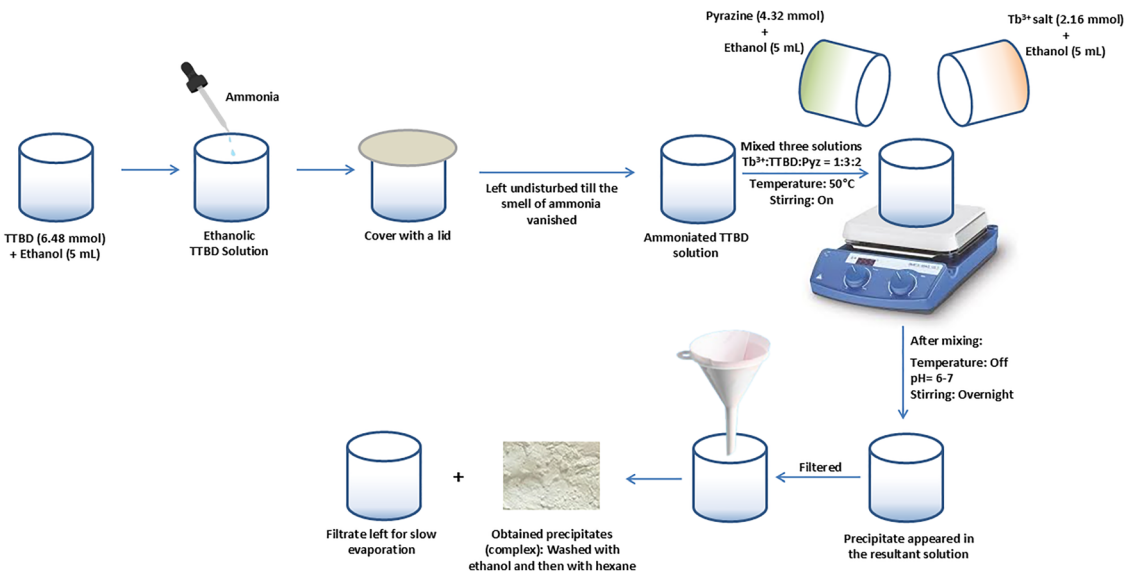

Fig. 2 Synthesis pathway for TbM.

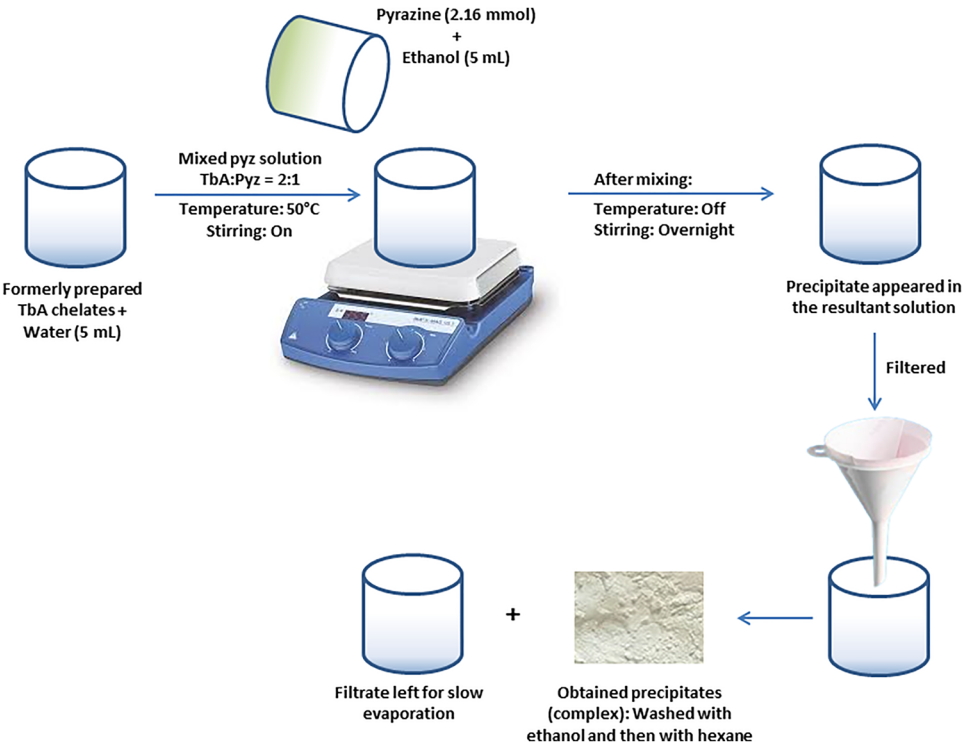

Fig. 3 Synthesis pathway for TbD.

Table 1 % CHN content (E and T) in TbA–TbD

Complex	Color	C_E (T)	H_E (T)	N_E (T)	Formula	Yield (%)
TbA	Beige	33.63 (33.58)	1.82 (1.88)	—	$C_{24}H_{16}TbF_9O_8S_3$	81
TbM	Beige	39.18 (39.11)	2.01 (2.05)	5.73 (5.70)	$C_{32}H_{20}TbF_9N_4O_6S_3$	76
TbD	Cream	36.14 (36.21)	1.69 (1.64)	1.67 (1.62)	$C_{52}H_{28}Tb_2F_{18}N_2O_{12}S_6$	72

the synthesized complexes are given in Table 1. The dinuclear complexes exhibited high hygroscopicity, with a water content of nearly 30%. Dinuclear complexes exhibit greater solubility in chloroform compared to their mononuclear counterparts. The incorporation of an additional Ln(TTBD)$_3$ unit in the dinuclear complex seems to enhance its solubility.[23]

4.2. IR study

Infrared (IR) spectroscopic analysis was conducted to detect any shifts in the vibrational wavenumbers of the ligands upon coordination with the trivalent terbium ion (Tb(III)) (Fig. S1–S3, SI). Significant IR spectral peaks corresponding to both free and coordinated ligands (TTBD and pyrazine) are listed in Table 2. Evidence of ligand coordination with Tb(III) ions is shown by the red-shift observed in the IR peaks of the resulting complexes. Notably, the peaks around 581 cm^{-1} and 459 cm^{-1} in the pyrazine-based complexes are tentatively attributed to Tb–N and Tb–O bond stretches, individually in accordance with the reported vibrational features of structurally related Tb(III) complexes.[24] Similar bands near ∼460 cm^{-1} and 580 cm^{-1} are assigned to Ln–O and Ln–N stretches in structurally related

Table 2 IR data of the free ligands and prepared complexes (in cm^{-1})

Complex	TTBD	Pyz	TbA	TbM	TbD
$\upsilon_{(Tb-O)}$	—	—	457	457	461
$\upsilon_{(Tb-N)}$	—	—	—	583	579
$\upsilon_{(C-F)}$	—	—	1137, 1189	1143, 1189	1140, 1184
$\upsilon_{(C-N)}$	—	—	—	1356	1324
$\upsilon_{(C=C)}$	—	1457	1462	1462	1464
$\upsilon_{(C=N)}$	—	—	—	1542	1543
$\upsilon_{(C=O)}$	1655	—	1609	1609	1609
$\upsilon_{(=CH)}$	—	—	2807	2838	2932

Tb(III) complexes.[25–28] In the binary complex (TbA), the Tb–O stretch is observed at ∼457 cm^{-1}. A considerable shift in C=O stretching vibration of the diketone group was also observed. In free TTBD, this stretch appears at ∼1655 cm^{-1},[29] shifting to around 1609 cm^{-1} after coordination, indicating its coordination with Tb(III) ions. In TbA, a large band due to asymmetric and symmetric O–H stretching confirms the presence of coordinated water molecules. Conversely, this band is absent in TbM and TbD, implying that water is replaced by pyrazine ligands and that the diketone coordinates to the metal ion through its oxygen

atom. All prepared complexes display strong IR peaks near 1463 cm^{-1} due to C=C stretching.[30] C=N stretching in the pyz-coordinated complexes (TbM and TbD) is observed at ~1542 cm^{-1}.[31] The IR profile of the ternary 1,3-diketonate complex includes C–N (1340 cm^{-1}) and enolic (=CH, ~2850 cm^{-1}) vibrations, whereas the enolic stretch in TbA is observed at ~2800 cm^{-1}. C–F stretching bands are shifted to lower wavenumbers, appearing at ~1140 (symmetric) and 1189 cm^{-1} (asymmetric), in both TbM and TbD, suggesting successful coordination between the metal and ligand. Due to strong IR absorptions from TTBD, most characteristic peaks of free pyrazine are hidden in the spectra of TbM and TbD. Nonetheless, a peak at ~1457 cm^{-1} in free pyrazine shifts to ~1463 cm^{-1} upon coordination.[32] In the case of TbM, coordination through a single nitrogen atom reduces the symmetry of the pyrazine molecule, leading to the presence of a new band in the 940–1010 cm^{-1} range.[33] A distinct band around 944 cm^{-1} in TbM, absent in TbD, further confirms monodentate coordination of pyrazine *via* one nitrogen atom.

4.3. ^{1}H-NMR study

PMR analysis was performed to ensure the preparation of the desired complexes TbA, TbM and TbD. The obtained results, listed in Table 3, are reliable with the existence of single and dual metal centers in (TbA, TbM) and (TbD), respectively. Free pyz showed a sharp singlet at 8.5 ppm,[34] whereas TTBD peaks were observed at δ 14.9, 7.84, 7.60, 7.20 and 6.45 ppm corresponding to the O–H proton, 3for the thienyl moiety and one for the methine proton, respectively.[35] PMR spectra of the complexes with paramagnetic metal ions are quite exciting as they induce large upfield or downfield shifts in the resonances of the coordinated diamagnetic chromophores. Signals of pyz and TTBD are shifted in opposite directions. Pyz protons shift upfield, while the methine protons of TTBD shift downfield. The NMR profile of TbM reveals four signals: two for TTBD and two for pyz. The relative intensity of the signals, *i.e.* 3 : 9 : 2 : 2 confirms the existence of two pyz units and three β-diketone moieties, making the metal ion octacoordinate. It is noteworthy that the Tb(III) ion induces large upfield paramagnetic shifts. PMRs in TbM span from −200 to 150 ppm. The appearance of two line-like peaks due to pyz and overall intensity ratio in TbM confirms the presence of two pyz units with a single $[Tb(TTBD)_3]$ unit in TbM, thus affirming its octacoordinated structure.

The NMR spectra of the dinuclear complex TbD (Tb–Tb) are particularly interesting, as the resonances are significantly shifted both upfield and downfield due to large magnetic anisotropy of these paramagnetic Ln(III) ions. This shift reflects the interaction among the unpaired electrons on the paramagnetic metal and the nuclear magnetic moments of the diamagnetic nuclei. In the TbD complex, the pyrazine protons experience an upfield paramagnetic shift appearing at −191.74 ppm (δ). A strong signal at 7.19–8.06 ppm (δ) is accredited to thienyl protons, and resonance at 145.05 ppm (δ), integrating for six protons, is due to the methine group. Terbium(III) is known to induce significant dipolar shifts and this causes the pyrazine resonances to shift upfield, showing a negative paramagnetic shift. However, the methine resonance is substantially shifted downfield. These combined upfield and downfield shifts in a specified complex confirm that the paramagnetic shifts result from dipolar interactions and the geometric factor $G = 3\cos^2\theta - 1/r^3$ plays an important role in altering the direction of shift.[36] The appearance of a single peak due to pyz along with the overall intensity ratio in TbD confirms the presence of only one pyz unit with two $[Tb(TTBD)_3]$ units in TbD, thereby affirming its seven-coordinated structure. TbA exhibits three signals: two due to TTBD (singlet for 3 =C–H protons at 108.21 accompanied by a multiplet (m) due to 9 thienyl protons in the 7.21–7.54 ppm region) and a signal due to complexed H_2O moieties. The changes in physical properties like solubility, along with the results from elemental, IR and NMR analyses, provide strong evidence supporting the formation of the desired complexes.

Table 3 PMR shifts of the prepared complexes (in ppm)

Complex	Peaks due to TTBD	Peaks due to pyz
Uncoordinated	14.9 (1H), 7.84 (1H), 7.60 (1H), 7.20 (1H), 6.45 (1H)	8.50 (4H)
TbA	108.21 (s), 7.21–7.54 (m)	1.53 (s)
TbM	116.19 (s), 7.13–7.81 (m)	−32.33 (s), −198.36 (s)
TbD	145.05 (s), 7.19–8.06 (m)	−191.74 (m)

4.4. UV analysis

Primary ligand TTBD displays two strong UV-absorption bands in the 225–280 nm range with maximum at 268 nm and 280–400 nm with maximum at 299 nm.[37] The electronic spectra of the prepared complexes predominantly feature intense π to π* transitions around ~275 nm, along with a more intense transition ~343 nm attributed to the TTBD ligand. The spectra of all complexes are similar, with absorption maxima around 343 nm. There is no observable transition in the visible region, which suggests that no metal-to-ligand charge transfer transitions occur. Coordination of the metal ion to the sensitizer results in the stabilization of π* orbitals of TTBD, which shifts their absorption to lower energy. This is illustrated in Fig. 4, where the electronic spectra of TTBD and the prepared complexes are overlapped at room temperature. Upon coordination with Tb(III) ions, a red-shift is observed in the spectra of the complexes. On the other hand, the pyz spectrum shows a single absorption band in the 200–275 nm range with a maximum at ~251 nm and a shoulder band at ~307 nm.[38] The spectrum of $[Tb(TTBD)_3(H_2O)_2]$ (TbA) mirrors that of the bridged bimetallic Tb(III) complex (TbD). However, this observed shift was more pronounced in the TbD spectrum, suggesting that when pyz coordinates to two $Tb(TTBD)_3$ units, the π* orbitals are further more stabilized and shifted to lower energy.[39] The electronic spectra of TbM and TbD are almost superimposable (Fig. 4), despite the difference in nuclearity. This similarity can be attributed to the presence of identical antenna ligands, namely TTBD and pyrazine. The comparable band shapes and the absence of any significant spectral shifts suggest that these ligands are the primary absorbers of UV-radiation and a Tb(III)

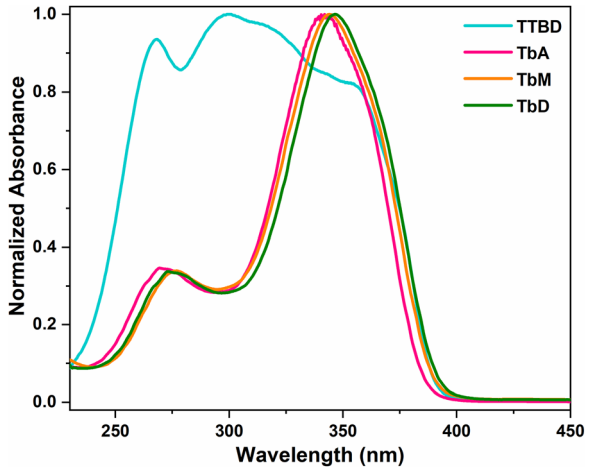

Fig. 4 Normalized electronic absorption graphs of TTBD and the prepared complexes.

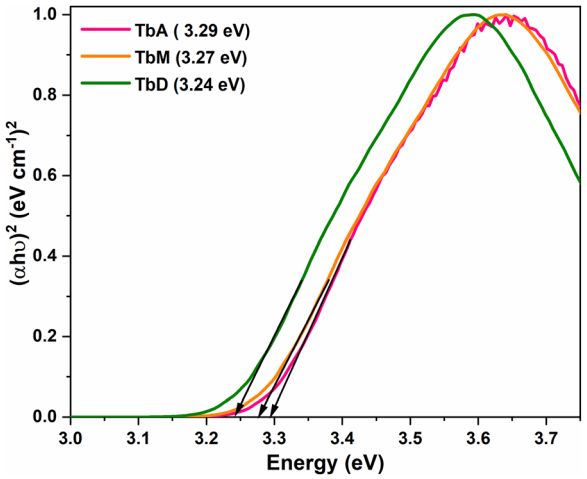

Fig. 5 Band-gap profiles of the prepared complexes.

ion itself contributes minimally to UV absorption, as evidenced by the lack of noticeable intraconfigurational f–f transitions within the recorded spectral range.

4.4.1. Band-gap determination. Coordination of the metal ion with the bridging moiety satisfies the high coordination requirement, promotes coordination saturation and enhances the thermal stability of dinuclear complexes. The optical band gap (E_g) of the prepared complexes was estimated with the help of electronic absorption data and Tauc's relation (eqn (1)).[40,41]

$$\alpha h\nu = A(h\nu - E_g)^n \quad (1)$$

Here, α is the molar absorption constant, $h\nu$ is the energy, A is the electronic tailing coefficient and n is the optical component. The $(\alpha h\nu)^2 \nu/s$ energy ($h\nu$) plot is drawn to estimate E_g and a tangent is drawn to the x-axis till the y-axis becomes zero. Fig. 5 depicts their obtained curves, and Table 4 constitutes the quantitative E_g data, which affirms the application of these complexes in semiconducting devices.[42] After careful assignment of the absorption edges, the order of the band gaps was established as TbD < TbM < TbA, consistent with the spectral features shown in Fig. 4. This order of band gaps can be rationalized by the structural features of the ligands. TbD, with its more extended π-conjugated system and stronger electronic delocalization, exhibits the narrowest band gap. TbM, which possesses moderate conjugation and orbital overlap, shows an intermediate band gap. In contrast, TbA, with a less delocalized electronic framework and more localized frontier orbitals, displays the largest band gap. Thus, the optical properties directly reflect the degree of conjugation and electronic communication within the ligand environment.

4.5. Photoluminescence spectroscopy

Optical excitation profiles of Tb(III) complexes were recorded by fixing the emission wavelength (λ_{em}) at 545 nm (Fig. 6(a)). These graphs reveal two intense bands corresponding to the $S_0 \rightarrow S_1$ and $S_0 \rightarrow S_n$ transition within the π system of the sensitizing ligands.[43] This prominent band is accompanied by a weaker band arising from transitions between the ground state ($^7F_6$) of the Tb(III) ion and its excited states ($^5D_3$, $^5G_{2-6}$, and $^5L_{6-10}$), centered around 390 nm.[44] The maxima of these bands appear at 245 and 275 nm for TbA, 240 and 276 nm for TbM, and 243 and 272 nm for TbD. After applying the Jacobian transformation (energy (eV) *vs.* intensity), the excitation spectra were re-analyzed (Fig. 6(b)) on the energy scale (eV). The corrected spectra reveal two distinct bands in the 200–300 nm region. Although weak shoulders may be present in this range, these do not separate into resolvable features under the present experimental conditions. Therefore, a two-band assignment best represents the observed spectral features. All complexes exhibit similar spectral profiles, although varying in intensity, due to differences in the number and nature of the absorbing groups.

Table 4 Some optical parameters of the prepared complexes

Complex	λ_{abs}	E_g	λ_{ex}	λ_{em}	Quantum yield	Lifetime
TbA	342	3.29	245, 275	546	04	0.073
TbM	344	3.27	240, 276	547	35	0.330
TbD	346	3.24	243, 273	546	23	0.259

PL emission profiles (Fig. 7) display four characteristic transitions due to $^5D_4 \rightarrow {}^7F_j$ transitions (j = 6–3) at ~489, 546, 590 and 615 nm, respectively. The Δj = +1 transition ($^5D_4 \rightarrow {}^7F_5$) is hyperintense and is attributed to a magnetic dipole transition, which dominates the whole spectrum and is particularly sensitive to changes in the coordination environment and mainly accountable for green emission.[45] The T_1 level of the TTBD diketone ligand lies at ~20 600 cm^{-1}, which is slightly above the emitting $^5D_4$ state of the Tb(III) ion (20 325 cm^{-1}).[46,47] However, the relatively small energy gap (275 cm^{-1}) may not be sufficient for highly efficient energy transfer, resulting in partial sensitization. Consequently, emission spectra include both sharp metal-centered peaks and broad ligand-based bands, indicating radiative decay from the ligands themselves and inefficient energy transfer to the metal center. The asymmetry

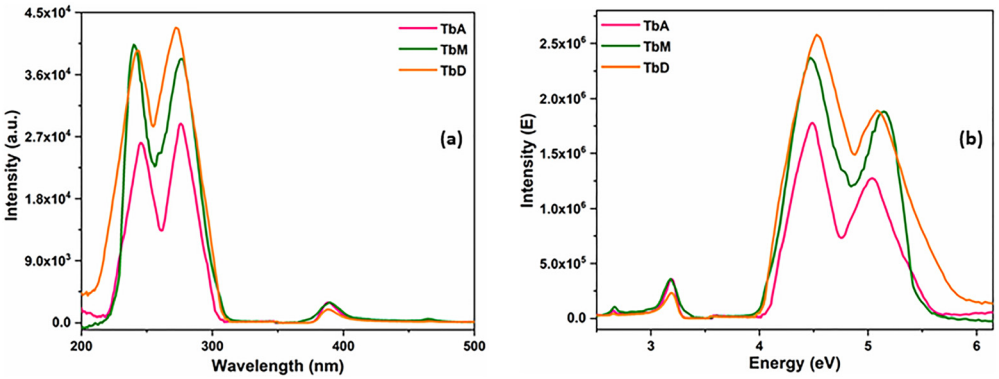

Fig. 6 (a) Excitation graphs of the prepared complexes in DCM. (b) Excitation spectra after Jacobian transformation, plotted on the energy scale (eV). Two distinct bands are clearly resolved in the 200–300 nm region. Minor shoulders are visible but do not evolve into independent bands under the present measurement conditions.

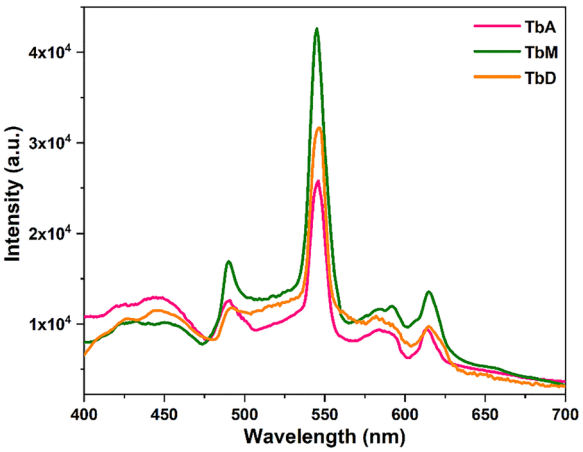

Fig. 7 Emission graphs of the prepared complexes in DCM.

ratio (R_A), which compares electric to magnetic dipole transition intensities, is 0.04 for TbA, 0.13 for TbM and 0.46 for TbD. Higher R_A values suggest a highly polarizable environment around the Tb(III) center in TbD in DCM.[48] Although the spectral shapes of all complexes are largely similar, as evident from the overlap in their profiles, the PL intensity of TbD is lower than that of TbM. This difference is likely due to fewer pyz groups coordinating to the Tb(III) center in TbD, limiting the energy transfer efficiency. Additionally, TbA shows reduced luminescence intensity due to high energy O–H oscillators within its coordination sphere, which act as quenchers.

4.5.1. Quantum yield. Photoluminescence quantum yield (PLQY), the ratio of photons emitted to photons absorbed, of the prepared complexes was determined in DCM.[49] This helped in analyzing the effect of the coordination environment on the photoluminescence intensity of the metal center. It was evaluated using eqn (2) against quinine bisulphate (reference) in dil. H_2SO_4 with a QY (Φ) equal to 0.546.[50,51]

$$\phi_s = \frac{\phi_r A_r I_r n_s^2}{A_s I_r n_r^2} \quad (2)$$

where the subscripts s and r represent the unknown sample and reference, respectively. I is the integrated intensity of emission, A is the absorbance at excitation wavelength and n is the refractive index. The notably high quantum yield value for TbM indicates a substantial sensitizing effect of pyz over TTBD for the Tb(III) ion in the prepared complexes. The quantum yield data are summarized in Table 4. The relative quantum yields are reported relative to a reference solution with a 10% error margin. The emission quantum yields for the complexes were found to be comparable to those reported previously for similar complexes.[52,53]

A study by R Ilmi and coworkers in 2015 reported that the PLQY of $[Tb(tfaa)_3]_2bpm$ (tfaa = trifluoroacetylacetone, bpm = 2,2′-bipyrimidine) in $CHCl_3$ is 48%. The quantum yield of TbM ($\Phi_{overall}$ = 35%) is significantly higher than that reported for $[Tb(hfa)_3(H_2O)_2]$ where hfa is hexafluoroacetylacetone ($\Phi_{overall}$ = 27%) and lower than that for $[Tb(thd)_3(H_2O)_2]$ where thd stands for the dipivaloylmethane complex ($\Phi_{overall}$ = 40%),[54] despite the fact that the magnitude of the $^5D_4$ lifetime of the TbM complex is not very high as compared to some of the recently reported highly luminescent Tb(III) complexes ($\Phi_{overall}$ = 56%; τ_{obs} = 2.63 ms).[55] However, there are reports of $\Phi_{overall}$ = 40% and τ_{obs} = 0.46 ms for Tb(III)–dipivaloylmethanato complexes.[54] Due to the electronic structure, Tb(III) has many levels, which can mix with the ligand wave functions, including a relatively low-lying 4f 5d state, which may explain why the lifetime is relatively short.[56]

4.5.2. Emission mechanism. To understand the emission mechanism in the prepared complexes, it is essential to study the energy transfer within these complexes. According to intramolecular energy transfer (IET), the efficiency of energy transfer depends on two main pathways: (i) the T_1 level of the chromophore transfers energy towards the emitting state of the metal ion *via* Dexter exchange interaction and (ii) the reverse energy transfer, which occurs owing to thermal deactivation.[57] Rate constants of these pathways are estimated by the ΔE value. PL profiles of the prepared complexes confirm that both pathways contribute to the IET process. According to the Dexter exchange theory of energy transfer,

the energy transfer rate constant (K_{ET}) is expressed by eqn (3).[58]

$$K_{ET} = \left(\frac{2\pi Z^2}{R}\right) e^{-2r/l} \int F_d(E) F_a(E) dE \quad (3)$$

where r is the distance between energy acceptor and donor, l is the van der Waals radius, and the integral shows the overlap between the excitation spectrum of the free sensitizer and the absorption profile of the complex. Here, $F_d(E)$ is the excitation spectrum of the sensitizer and $F_a(E)$ is the absorption spectrum of Tb(III) ions in the prepared complexes, while $2\pi Z^2/R$, r and l are constants during the IET process. From eqn (3), it can be inferred that the energy transfer rate constant (K_{ET}) is directly related to the overlap integral of $F_d(E)$ and $F_a(E)$. Therefore, a decrease in ΔE results in an increased overlap between the excitation profile of the donor and the absorption profile of the acceptor, leading to enhanced energy transfer. However, chromophores with high ΔE do not effectively sensitize Ln(III) ions due to the small overlap integral, which results in inefficient K_{ET}. On the other hand, very less ΔE also leads to inefficient energy transfer from the sensitizer to the metal ion due to B_{ET} (back energy transfer), which causes luminescence quenching. Therefore, it is concluded that ΔE has reverse effects on the abovementioned two energy transfer pathways, and there is an optimal ΔE range of approximately 3000 ± 500 cm^{-1}.[59] In the prepared complexes, pyz has higher T_1 states compared to TTBD, making it a better candidate for sensitizing the Tb(III) ion. Data presented in Table 5 indicate that energy transfer from TTBD to the Tb(III) ion is quite inefficient (Fig. 8), resulting in low emission intensity for TbA and TbD. This inefficiency is due to the minimal energy difference between the chromophores in these complexes and the emitting level of the metal center, which leads to vibrationally assisted energy transfer and ultimately to B_{ET}. This explains the presence of a wide ligand-based band in the emissive pattern of these complexes. The T_1 level of TTBD is slightly above the $^5D_4$ state of the Tb(III) ion, which accounts for the intense ligand-based band observed in TbA and TbD. This band suggests that the sensitizer ligands released a significant portion of the absorbed energy non-radiatively. Additionally, out of all prepared complexes, TbM displayed the most intense emission due to the presence of two pyz moieties per Tb(III) ion, further demonstrating that pyz is a better sensitizer among the chosen ligands. Despite an inadequate ΔE value and the presence of a large, intense ligand-based band, the complexes still exhibit significant photoluminescence intensity. This affirms that some of the absorbed UV energy might be transferred from the S_0 state of the sensitizer to its T_1 state and subsequently to the Tb(III) ion or from the T_1 state of the ligand to a higher excited state of the metal ion (Fig. 9).[60]

Table 5 T_1 energy with its difference with the emitting level of the central ion

Complex	Energy (cm^{-1})
E_{pyz}	26820
E_{TTBD}	20600
$E_{Tb(III)}$	20325
$\Delta E_{TTBD-Tb(III)}$	275
$\Delta E_{Pyz-Tb(III)}$	6495

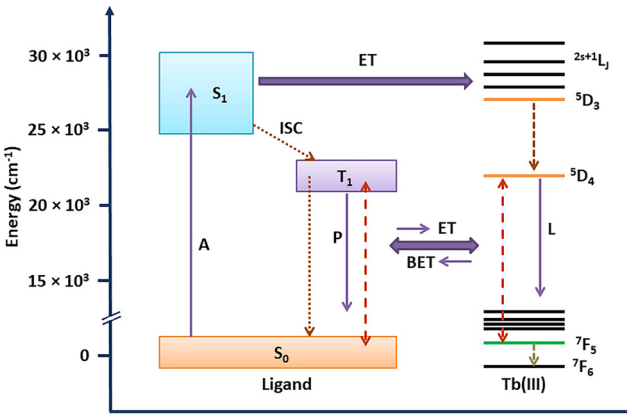

Fig. 8 Schematic diagram of probable energy transfer occurring in TbA–TbD.

4.5.3. Decay time. The fluorescence decay time plays a dynamic role in practical implication of luminescence-based techniques, including fluorescence resonance energy transfer (FRET).[61] The emission lifetimes of the prepared complexes were measured using time-resolved luminescence spectroscopy at their respective λ_{ex} and λ_{em}. Decay profiles corresponding to the $^5D_4$ emitting level of the Tb(III) ions are well-described by a single-exponential fit (Fig. S4, SI), suggesting either the presence of a single type of emitting species or multiple ions occupying nearly identical coordination surroundings.[62] In other words, the obtained decay curves indicate a dominant single emissive environment and a single relaxation pathway from the $^5D_4$ excited state. Furthermore, no physical interpretation is assigned to the minor fluctuations in the decay curves. The determined luminescence lifetimes (in ms) of TbA, TbM and TbD in the solid state are 0.073, 0.330 and 0.259, respectively. Logarithmic decay time profiles of TbA–TbD are displayed in Fig. 10. The lifetime value of the present complex TbM is longer than those reported for similar Tb(III) complexes, $[Tb(L)_3(phen)]_2$ (173.13 ns) where phen = 1,10-phenanthroline,[63] and $[Tb(fod)_3(phen)]$ (0.23 ms) where fod = 6,6,7,7,8,8,8-heptafluoro-2,2-dimethyl-3,5-octanedione,[64] and shorter than those for $[Tb(dbm)_3(impy)]$ (t_1 = 1.45 ms, t_2 = 12.99 ms)[65] where dbm is dibenzoylmethane and impy = imidazo[5-*a*]pyridin-3-ylidene, $[Tb(fod)_3(m\text{-}bpp)Tb(fod)_3]$ (2.04 ms) where m-bpp is bis(pyrazolyl)pyridine,[66] $[Tb(L)(tfac)_2]$ (0.34 ms) where tfac is 3-trifluoroacetylcamphorato, $[Tb(DBM)_3(TPPO)]$ (t_1 = 0.8946 ms, t_2 = 0.0214 ms) where TPPO is triphenylphosphine oxide[67] and $[Tb(dbm)_3(HMPA)]$ (t_1 = 1.0499 ms, t_2 = 0.0508 ms) where HMPA is hexamethylphosphoramide.[67] These data are very well justified by the energy gap existing between the triplet state of the sensitizer and the emissive state of the central metal ion.

4.5.4. Color modulation. The emissive color of the synthesized complexes is governed by three dimensionless parameters

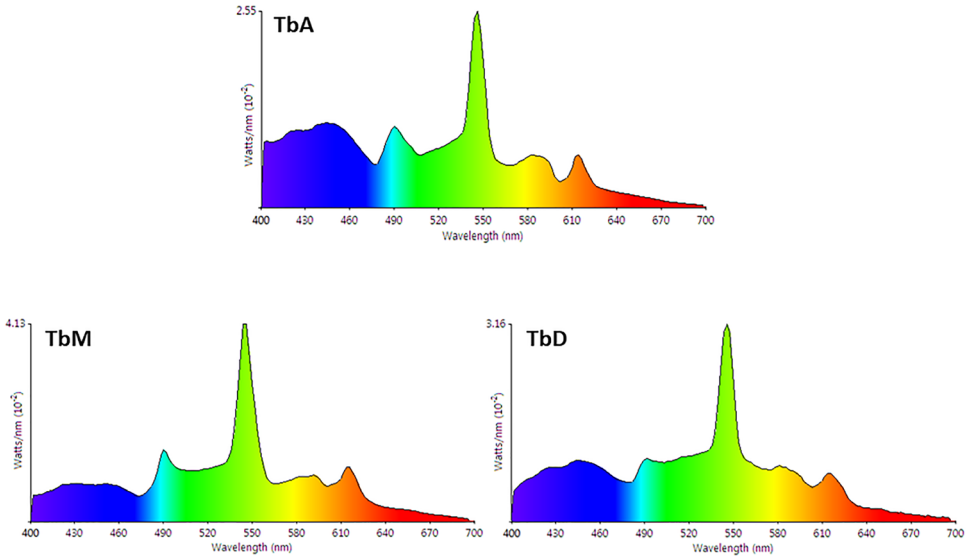

Fig. 9 Color contribution of each peak towards emissive color in TbA–TbD.

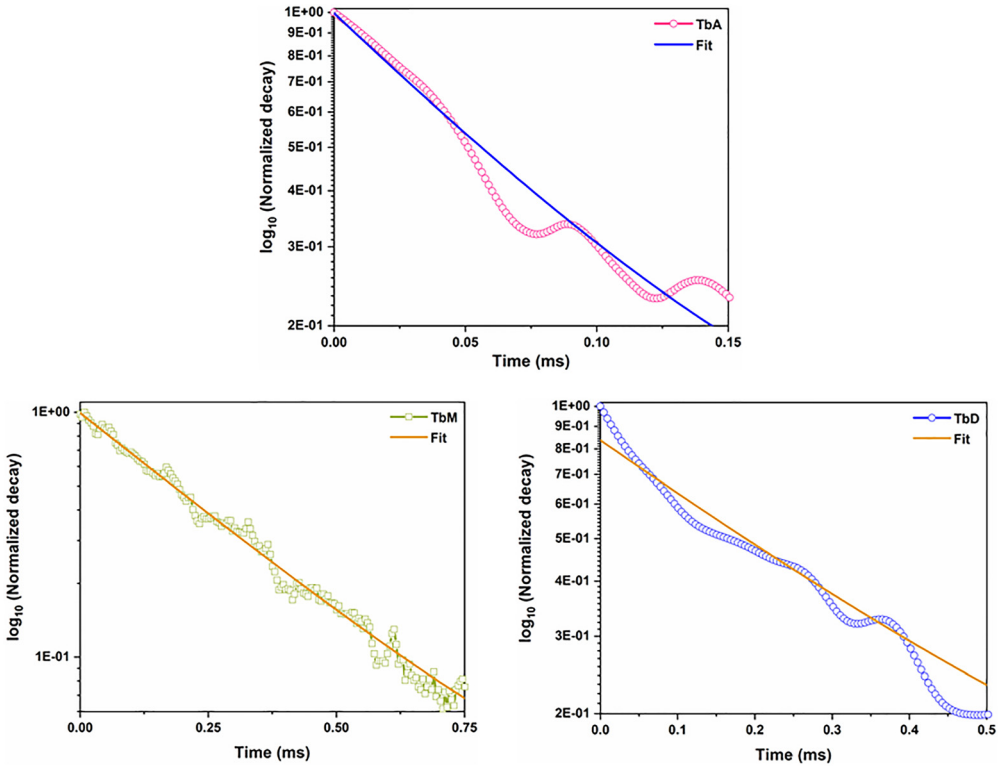

Fig. 10 Logarithmic decay time profiles of TbA–TbD.

used to calculate x and y color coordinates within the 1931 CIE color triangle. CIE diagrams derived from PL spectra are presented in Fig. 11. CIE color gamut analysis shows that variations in nuclearity and the nature of the coordinated chromophores significantly influence the observed emission colors. Notably, the intensity and wavelength of luminescence vary among the complexes. For instance, the binary complex TbA shows a markedly strong residual fluorescence (I_B), which reflects substantial non-radiative decay caused by coordinated solvent molecules. This results in a blue-shifted emission and a pronounced deviation from the characteristic green luminescence typically observed in ternary Tb(III) complexes. Color tunability is evident in these systems: emissive color transition from characteristic green to yellow-white and bluish-white for

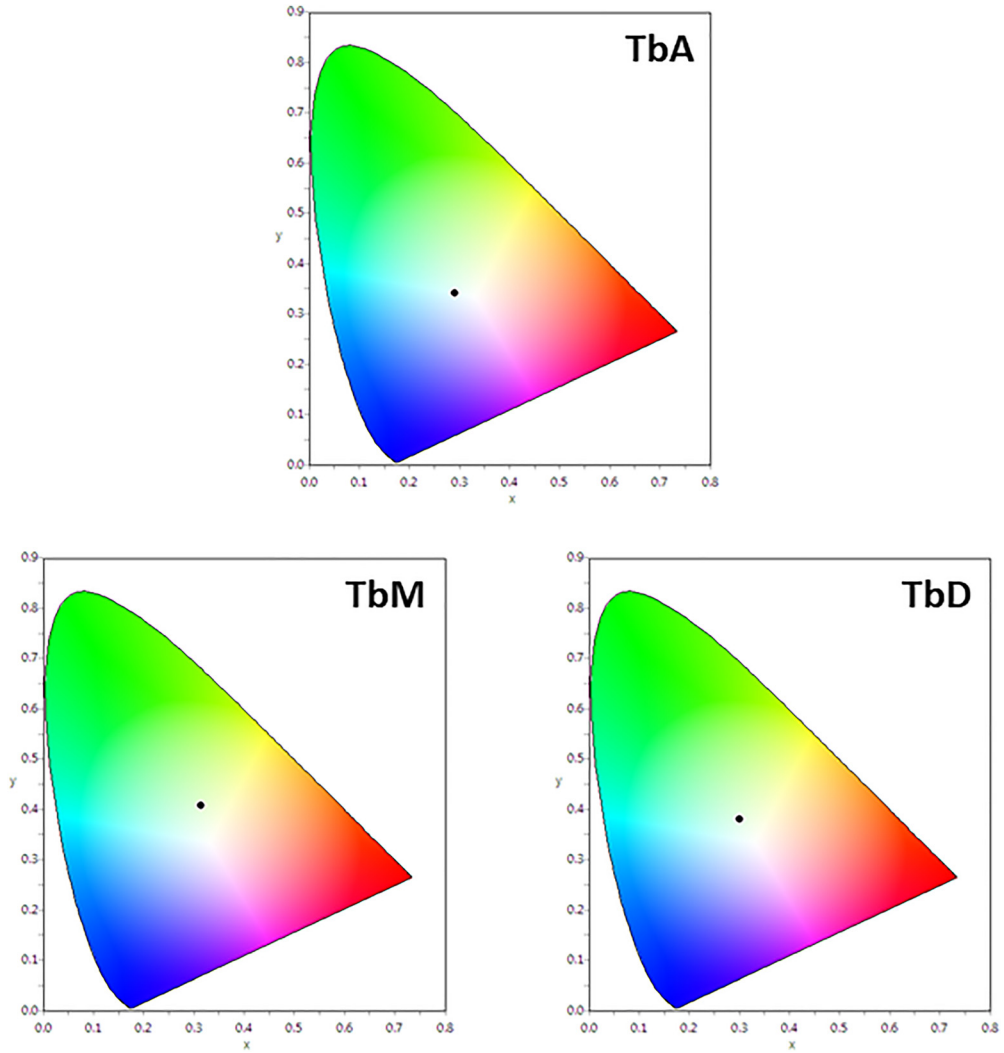

Fig. 11 CIE 1931 (*x*, *y*) plot of TbA, TbM and TbD.

TbD, TbM and TbA, respectively. This shift is attributed to differing energy transfer mechanisms. At higher excitation energies, the antenna effect becomes more dominant, enhancing green emission in the Tb(III) complexes.[68] On the contrary, when energy absorption is insufficient to drive ISC efficiently, residual fluorescence (F_R) predominates, especially in the blue spectral range, contributing to near-white light emission in some complexes. The CIE diagram (Fig. 11) visually confirms the emission colors of the complexes. Moreover, the photograph of the powder emission under UV excitation has also been added in Fig. S5 (in the SI) to provide direct visual confirmation of the emission color. By modulating the relative intensities of the green emission band (I_A) from Tb(III) ions and blue emission (I_B), it is possible to fine-tune the overall luminescent output. This tunability offers a promising way of achieving white light emission, suggesting that these materials have potential applications in fabricating wLE (white-light emitting) devices or red-green-blue (RGB) emissive elements for photonic technologies.[69] Moreover, their ability to emit across a wide range of the visible spectrum with different sensitizers makes them strong candidates for use as color indicators.[69] Color coordinates *x*, *y* and *u*′, *v*′ are listed in Table 6.

4.5.5. Judd–Ofelt (J–O) calculation. The Judd–Ofelt concept is a theoretical framework that helps to explain the PL features of Ln(III) ions in solid state environments. It delivers a quantitative understanding of how the coordination surrounding influences the emissive peaks of these ions. According to this, ligand field interactions between Ln(III) ions and the sensitizer exist and transitions among the energy levels of the ions are mainly allowed as magnetically dipole (MD) transitions.[70] It quantifies the strength of these peaks through three parameters, namely, Ω_2, Ω_4 and Ω_6. This theory is widely applied in the development and optimization of photonic materials for devices like lasers.[71]

Table 6 (*x*, *y*) and (*u*′, *v*′) values of the prepared complexes

Complex	TbA	TbM	TbD
x, *y*	0.290, 0.340	0.314, 0.407	0.301, 0.380
u′, *v*′	0.178, 0.471	0.173, 0.505	0.173, 0.491

Absorption spectra of TbA, TbM and TbD were measured in the near-infrared region (900–2900 nm) using the DCM solvent in the liquid form. The spectra of TbM and TbD are displayed, because similar spectra for TbA are obtained with slightly lower intensity. The observed absorption profiles showed spin-allowed, but parity-forbidden, narrow f–f absorption peaks, arising from the ground state of Tb(III) ions ($^7F_6$) and transitioning to various excited states. These profiles revealed five transitions from the $^7F_6$ ground state to the $^7F_0$, $^7F_1$, $^7F_2$, $^7F_3$ and $^7F_4$ states, occurring at 1668 nm, 1907 nm, 1980 nm, 2148 nm and 2730 nm, respectively. To determine the J–O parameters (Ω_2, Ω_4, Ω_6), calculations were carried out based on the obtained NIR absorption data.[72] These transitions were assigned following the work of Carnall and team and the strength of the absorption transitions was expressed as oscillator strength calculated using eqn (4).[73]

$$f_{\text{exp.}} = \frac{2.303mc^2}{N_A\pi e^2}\int \varepsilon(\bar{\nu})\cdot \mathrm{d}\bar{\nu} = 4.319\times 10^{-9}\ (\text{mol cm}^2\ \text{l}^{-1})\int \varepsilon(\bar{\nu})\cdot \mathrm{d}\bar{\nu} \quad (4)$$

In this context, $\varepsilon(\bar{\nu})$ refers to the molar absorptivity at the corresponding ($\bar{\nu}$) wavenumber in cm^{-1}. It can be determined by calculating the area under the curve of the specific peak shown in Fig. 12. Intensity of the ED transitions, originating from the ground state ($^7F_6$), is calculated using eqn (5).[73]

$$f_{\text{calc.}} = \frac{8\pi^2 mc}{3h\lambda(2J+1)n^2}\frac{n(n^2+2)^2}{9}\sum_{t=2,4,6}\Omega_t\left|\langle\phi_J|U^t|\phi'\rangle_J\right|^2 \quad (5)$$

Here, π, m, c and h maintain their standard denotations, λ represents the wavelength of absorption transition and $(2J + 1)$ refers to the spin multiplicity of the ground J level, while n denotes the refractive index. $\|U_t\|^2$ is the irreducible reduced matrix element, where t can be 2, 4 or 6. This term is associated with the coupling of the peak between the ground and excited states and is insensitive to the coordinated chromophores. Data for these elements were sourced from the work of Carnall and team.[74] The J–O theory describes both magnetic (MD) and electric dipole (ED) transitions; however, MD peaks are generally negligible when calculating oscillator strength. Therefore, only ED transitions are used to determine the oscillator strength. The theoretical and experimental oscillator strength results are summarized in Table 7. The literature has revealed a strong connection between absorption and f_{calc}. As a result, the intensity parameters (Ω_2, Ω_4, and Ω_6) are determined by equating the theoretical and experimental oscillator strengths (eqn (6)).[73]

Table 7 Oscillator strength and J–O features of the prepared complexes

Transitions	TbA		TbM		TbD	
$^7F_6$ →	$f_{\text{exp.}}$	$f_{\text{calc.}}$	$f_{\text{exp.}}$	$f_{\text{calc.}}$	$f_{\text{exp.}}$	$f_{\text{calc.}}$
$^7F_0$	0.86	0.79	0.97	1.11	1.06	1.09
$^7F_1$	0.93	0.98	1.07	0.91	1.23	0.96
$^7F_2$	0.21	0.27	0.36	0.41	0.58	0.52
$^7F_3$	1.02	1.01	1.15	1.34	0.99	1.01
$^7F_4$	0.87	0.83	1.64	1.57	1.76	1.68
Ω_2 ($\times 10^{-20}$ cm^2)	5.913	—	6.126	—	6.003	—
Ω_4 ($\times 10^{-20}$ cm^2)	0.841	—	1.537	—	0.342	—
Ω_6 ($\times 10^{-20}$ cm^2)	2.912	—	3.116	—	3.537	—

$$f_{\text{exp}} \leftrightarrow f_{\text{calc}} = \frac{8\pi^2 mc}{3h\lambda(2J+1)n^2}\frac{n(n^2+2)^2}{9} \times \left[\left(\Omega_2\left|\langle\varphi_J|U^2|\varphi'\rangle_J\right|^2\right) + \left(\Omega_4\left|\langle\varphi_J|U^4|\varphi'\rangle_J\right|^2\right) + \left(\Omega_6\left|\langle\varphi_J|U^6|\varphi'\rangle_J\right|^2\right)\right] \quad (6)$$

The intensity parameters (Ω_2, Ω_4, and Ω_6) for the TbA, TbM and TbD complexes are provided in Table 7. The order of these parameters for the complexes is $\Omega_2 > \Omega_6 > \Omega_4$. The largest value of Ω_2, compared to Ω_4 and Ω_6, suggests the existence of a covalent bond among the Tb(III) and –O atoms, alongside a notably asymmetric environment and a strong ligand field around the Tb(III) ions. Moreover, Ω_6 and Ω_4 offer valuable understandings of the viscosity as well as the structural rigidity of the Tb(III) complexes.[75] Radiative transition probability is an essential factor for assessing the emissive energy of complexes when irradiated with UV-radiation. It is calculated using J–O parameters (eqn (7)).[76]

$$A_{\text{rad.}} = \frac{64e^2\pi^4}{3h(2J+1)\lambda^3}\frac{n(n^2+2)^2}{9}[S_{\text{ED}} + S_{\text{MD}}] \quad (7)$$

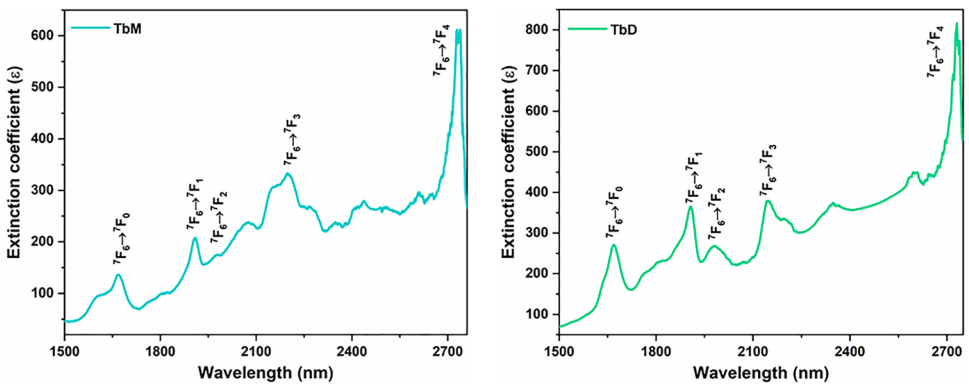

Fig. 12 NIR UV-absorption profiles of TbM and TbD.

Here, the intensity of the ED and MD transitions is represented as S_{ED} and S_{MD}, respectively. The contribution of S_{MD} is neglected in calculation, leading to the following simplified eqn (8).[73]

$$A_{rad.} = \frac{64e^2\pi^4}{3h(2J+1)\lambda^3}\frac{n(n^2+2)^2}{9}S_{ED} \quad (8)$$

The strength of ED transitions (S_{ED}) is expressed in eqn (9).[73]

$$S_{ED} = \sum_{t=2,4,6}\left(\Omega_t\left|\langle\phi_J|U^t|\phi'\rangle_J\right|^2\right) \quad (9)$$

Matrix values used here are sourced from ref. 77 and the resulting radiative features are presented in Table 8. The radiative decay lifetime for the TbM and TbD complexes is determined by the reciprocal of total radiative rate.[73] Overall radiative probability is the sum of the probabilities for each transition arising from $^5D_4$ in the emission profile. Quantitative data of the total radiative rate (A_{rad}), non-radiative rate (A_{nrad}) and radiative decay lifetime (τ_{rad}) are summarized in Table 9. These parameters show higher values for the TbD complex due to the presence of an additional metal center. This affirms that both metal ions contribute to the radiative relaxation, thus improving the luminous efficiency of the prepared complexes.

4.6. Thermal analysis

FTIR spectra indicate the presence of coordinated water molecules in TbA; however, this technique alone cannot provide quantitative information. To address this, TGA analysis was performed for all three prepared complexes. In the TbA thermogram (Fig. 13), the initial weight loss observed between 111 and 257 °C corresponds to the release of coordinated water molecules, consistent with the FTIR results. The curve shows that TbA loses mass in three steps. The first degradation stage of this binary complex is related to the loss of water and corresponds to the weight loss of 20.83% (theor. = 22.36%). The percentage of weight loss allows the release of two molecules of water, which aligns well with the proposed structure. This complex is stable up to about 237 °C. The other two degradation stages are connected with the dissociation of TTBD from the metal ion. Finally, at 541 °C, the stable oxide of Tb(III) ions is obtained (Tb_2O_3) with a total mass loss of 79.04% (theor. = 81.84%).

The thermal behavior of the prepared complexes was investigated over a temperature range of 30–600 °C using thermogravimetric analysis (TGA). All the complexes exhibited similar thermal decomposition profiles. The weight loss profile for the TbM and TbD showed two-step weight loss as presented in Fig. S6 (in the SI). The TG curve of TbM showed an initial

Table 9 Radiative parameter of the prepared complexes

Property (ms^{-1})	TbA	TbM	TbD
Total $A_{rad.}$	416.04	520.08	440.21
$A_{nrad.}$	0.284	0.219	0.226
$\tau_{exp.}$	0.073	0.330	0.259
$\tau_{rad.}$	0.357	0.549	0.485

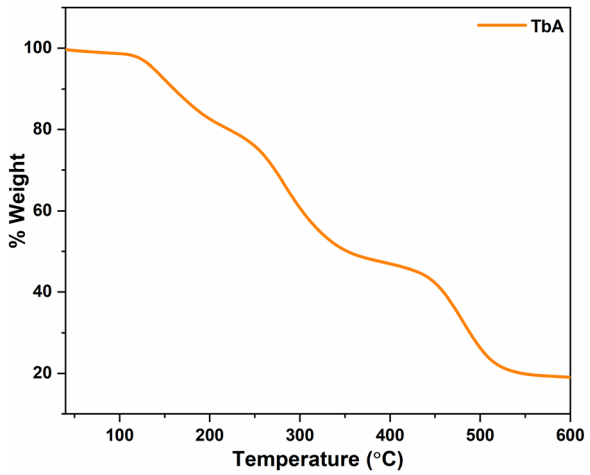

Fig. 13 TG profiles of TbA.

18.75% (theor. 16.18%) decomposition until 364 °C due to the loss of two pyz molecules. The major second decomposition event occurred at around 450 °C (62.05% mass loss, reaching 16.14%), which is attributed to the degradation of the TTBD ligands (occurring in the 450–560 °C range) (theor. weight loss 83.7%). In comparison, the thermal decomposition temperatures of TbD were lower than those of the mononuclear complexes. Thereby, compared to the dinuclear Tb(III) complex with a pyrazine spacer (bridging ligand), the currently synthesized mononuclear Tb(III) complexes exhibit higher thermal stability. Upon comparing the thermal stability of TbA with TbM, the latter is found to have higher stability as the binary complex possesses coordinated water moieties and starts decomposing around 120 °C.

4.7. Computational modeling

The molecular structures of the synthesized complexes were generated using Avogadro software, with energy minimization ($dE = 0$) achieved through automatic optimization tools.[78] The geometry of these molecules was optimized at the BP/def2-SVP (DFT level) and def2-SVP (basis set) levels.[79]

Table 8 β and A_{rad} of specific peaks of the prepared complexes

	TbA	TbM (solid)	TbD (solid)	$A_{rad.}$ (JJ') (TbA)	$A_{rad.}$ (JJ') (TbM)	$A_{rad.}$ (JJ') (TbD)
β ($^5D_4$ to $^7F_6$)	0.039 (0.111)	0.095 (0.102)	0.266 (0.249)	76.43	87.51	72.62
$^7F_5$	0.920 (0.878)	0.714 (0.790)	0.573 (0.560)	268.71	343.82	295.43
$^7F_4$	0.016 (0.021)	0.069 (0.103)	0.046 (0.011)	33.87	42.76	36.17
$^7F_3$	0.024 (0.019)	0.120 (0.016)	0.114 (0.209)	37.03	45.99	35.99

A large core quasi-relativistic effective core potential was utilized due to the deeply buried f-orbitals and their negligible contribution to metal–ligand interactions. DFT modeling was performed *via* both ORCA and Avogadro software.[80–82] After energy minimization, this file was used as an input in ORCA for further calculations,[83] which

Table 10 Iso-structural surfaces with energy in the prepared complexes

LUMO+1	(-1.873)	(-2.159)	(-2.431)
LUMO	(-3.196)	(-3.279)	(-3.380)
HOMO	(-6.497)	(-6.546)	(-6.613)
HOMO−1	(-7.124)	(-7.379)	(-7.992)
Complex	TbA	TbM	TbD

Table 11 Global reactivity descriptors of the prepared complexes

Complex	I.E.	E.A.	χ	H	σ	μ
TbA	6.497	3.196	4.846	1.650	0.605	-4.846
TbM	6.546	3.279	4.912	1.633	0.612	-4.912
TbD	6.613	3.380	4.996	1.616	0.618	-4.995

generated an output file that allowed the presentation of energy and structure of frontier molecular orbitals (FMOs) in Avogadro (Table 10). The energy gap between the HOMO and LUMO energy levels provided theoretical band gap data, which showed strong agreement with experimentally obtained band gap data (from UV study). These outcomes validate the reliability of the employed computational methods. The band gap values in the 3.2–3.3 eV range suggest the potential of these complexes for photonic applications. According to Koopmans' theorem, ionization energy (I.E.) corresponds to the energy of the HOMO level, while electron affinity (E.A.) relates to the LUMO energy level (eqn (10), allowing for the calculation of various global reaction parameters.[84] From the DFT calculations, global reaction descriptors such as chemical hardness (η), ionization potential (μ), electronegativity (χ), Fukui functions and softness (σ) were derived (eqn (11)).[85] These descriptors tell about the chemical reactivity and stability of the system, as well as its ability to undergo redox reactions during chemical reactions. These are useful in designing and optimizing the reaction, identifying reactive sites, predicting reaction rates and assessing the possibility of undesirable side products. Global reaction parameters are summarized in Table 11.

$$\text{I.E.} = -E_{\text{HOMO}}, \quad \text{E.A.} = -E_{\text{HOMO}} \tag{10}$$

$$\chi = \frac{\text{I.E.} + \text{E.A.}}{2}, \quad = \frac{\text{I.E.} - \text{E.A.}}{2}, \quad \sigma = \frac{1}{\eta}, \quad \mu = -\chi \tag{11}$$

Among the three prepared complexes, TbD demonstrates the highest ionization energy at 6.613 eV, whereas TbM and TbA show slightly lower values of 6.546 eV and 6.497 eV, respectively. In a similar trend, TbD also exhibits the highest electron affinity (3.380 eV), followed by TbM (3.279 eV) and TbA (3.196 eV). Based on these ionization energy and electron affinity values, electronegativities were calculated using Mulliken's scale, following the order: TbD (4.996 eV) > TbM (4.912 eV) > TbA (4.846 eV). Chemical hardness, derived from the difference between I.E. and E.A., indicates that TbA (1.650) is the most chemically stable, while TbD (1.616) is the least. Conversely, TbD shows the highest chemical softness (0.618), suggesting that it is the most reactive, with TbA (0.605) being the least reactive. These results collectively imply that the TbA (binary complex) is the most stable and chemically inert, whereas TbD (dinuclear complex) is the most reactive and least stable of the three complexes.

5. Conclusions

Three Tb(III) complexes, namely TbA, TbM and TbD, were synthesized using the ligand 4,4,4-trifluoro-1-(2-thienyl)-1,3-butanedione (TTBD) and a fluxidentate sensitizer pyrazine (pyz). Structural analyses (CHN, IR and NMR) revealed that TbA and TbM are mononuclear and isostructural, while TbD forms a dinuclear structure with pyrazine acting as a spacer ligand. Their photoluminescent behavior was investigated through UV-visible absorption, PL spectroscopy and time-resolved emission measurements. All complexes displayed characteristic terbium(III) emission along with a prominent ligand-based band, attributed to the energy mismatch with the sensitizing ligands. Introduction of the chosen chromophores led to a marked shift in emission color from green to near-white. The Judd–Ofelt theory was applied to support the experimental photophysical findings. Radiative lifetimes and energy transfer rates were estimated from the luminescence decay profiles. Furthermore, electronic absorption data analyzed *via* Tauc's method, supported by computational DFT calculations, indicated semiconducting properties with optical band gaps near 3.2 eV. The dual features of near-white emission and semiconducting behavior suggest their strong potential for applications in optoelectronic and photonic devices although detailed photostability studies have not yet been conducted and will be the subject of future investigations. Thereby, the use of pyrazine as a co-ligand effectively fine-tunes the luminescence output of Tb(III) complexes.

Author contributions

Vandana Aggarwal = data curation and writing – original draft; Devender Singh = writing – review and editing and supervision; Anuj Dalal = investigation; Vandna Nishal = visualization; Sumit Kumar = resources; Rajender Singh Malik = validation; Parvin Kumar = conceptualization; Jayant Sindhu = formal analysis; Varun Kumar = software.

Conflicts of interest

The authors declare that they have no conflicts of interest.

Data availability

The authors affirm that the information/data of this research article is available within the article.

Supplementary information (SI) is available. See DOI: https://doi.org/10.1039/d5ma01145k.

Acknowledgements

Vandana Aggarwal is thankful to UGC-New Delhi for providing a JRF [221610012377].

References

1 P. Kumar, P. Kalita, M. A. Palacios, V. Kumar, J. Acharya, E. Colacio and V. Chandrasekhar, Synthesis, structures and magnetic studies of hexanuclear lanthanide complexes:

SMM behavior of the DyIII analogue and MCE properties of the GdIII analogue, *Dalton Trans.*, 2023, **52**, 10594–10608, DOI: 10.1039/D3DT01489D.

2 D. Singh, S. Bhagwan, R. K. Saini, V. Nishal and I. Singh, Development in organic light-emitting materials and their potential applications, *Adv. Magn. Opt. Mater.*, 2016, **32**, 473–519, DOI: 10.1002/9781119241966.

3 V. Aggarwal, D. Singh, S. Malik, S. Bhagwan, S. Kumar, R. S. Malik, P. Kumar and J. Sindhu, Highly emissive dinuclear europium (iii) complex with heteroaryl β-diketone and fluxidentate pyrazine: dual role as UV converters and semiconductors, *RSC Adv.*, 2025, **15**, 44102–44115, DOI: 10.1039/D5RA06968H.

4 C. Wang, G. Xu, W. Wang, Z. Ren, C. Zhang, Y. Gong, M. Zhao, Y. Qu, W. Li, H. Zhou and Y. Q. Li, Bioinspired hot-spot engineering strategy towards ultrasensitive SERS sandwich biosensor for bacterial detection, *Biosens. Bioelectron.*, 2023, **237**, 115497, DOI: 10.1016/j.bios.2023.115497.

5 V. Aggarwal, D. Singh, A. Hooda, S. Malik, S. Dalal, S. Redhu, S. Kumar, R. S. Malik and P. Kumar, Comprehensive investigation of ternary dysprosium complexes for white light emission: Synthesis, spectroscopic and colorimetric analyses, *J. Lumin.*, 2024, **270**, 120555, DOI: 10.1016/j.jlumin.2024.120555.

6 J. Li, Y. Zhao, D. Yu and C. Zhan, Recent Advances in d-f Transition Lanthanide Complexes for Organic Light-Emitting Diodes: Insights Into Structure–Luminescence Relationships, *Laser Photonics Rev.*, 2025, 2402198, DOI: 10.1002/lpor.202402198.

7 S. I. Weissman, Intramolecular energy transfer the fluorescence of complexes of europium, *J. Chem. Phys.*, 1942, **10**, 214–217, DOI: 10.1063/1.1723709.

8 A. Masuya-Suzuki, S. Goto, R. Nakamura, R. Karashimada, Y. Kubota, R. Tsunashima and N. Iki, Emergence of the super antenna effect in mixed crystals of ytterbium and lutetium complexes showing near-infrared luminescence, *RSC Adv.*, 2022, **12**, 30598–30604, DOI: 10.1039/D2RA06007H.

9 M. Latva, H. Takalo, V. M. Mukkala, C. Matachescu, J. C. Rodríguez-Ubis and J. Kankare, Correlation between the lowest triplet state energy level of the ligand and lanthanide(III) luminescence quantum yield, *J. Lumin.*, 1997, **75**, 149–169, DOI: 10.1016/S0022-2313(97)00113-0.

10 A. Dalal, K. Nehra, A. Hooda, D. Singh, P. Kumar, S. Kumar, R. S. Malik and B. Rathi, Luminous lanthanide diketonates: Review on synthesis and optoelectronic characterizations, *Inorganica Chim. Acta.*, 2023, **550**, 121406, DOI: 10.1016/j.ica.2023.121406.

11 K. Nehra, A. Dalal, A. Hooda, S. Bhagwan, R. K. Saini, B. Mari, S. Kumar and D. Singh, Lanthanides β-diketonate complexes as energy-efficient emissive materials: A review, *J. Mol. Struct.*, 2022, **1249**, 131531, DOI: 10.1016/j.molstruc.2021.131531.

12 D. Singh, V. Tanwar, S. Bhagwan and I. Singh, Recent advancements in luminescent materials and their potential applications, *Adv. Magn. Opt. Mater.*, 2016, 317–352, DOI: 10.1002/9781119241966.

13 R. Ilmi, D. Zhang, J. D. Dutra, N. Dege, L. Zhou, W. Y. Wong, P. R. Raithby and M. S. Khan, A tris β-diketonate europium(III) complex based OLED fabricated by thermal evaporation method displaying efficient bright red emission, *Org. Electron.*, 2021, **96**, 106216, DOI: 10.1016/j.orgel.2021.106216.

14 Z. Ahmed and K. Iftikhar, Efficient layers of emitting ternary lanthanide complexes for fabricating red, green, and yellow OLEDs, *Inorg. Chem.*, 2015, **54**, 11209–11225, DOI: 10.1021/acs.inorgchem.5b01630.

15 B. Jia, Y. Liu, X. Geng, Y. Li, C. Zhang, Y. Qu, X. Liu, M. Zhao, Y. Yang, W. Li and Y. Q. Li, Deciphering the Physical Binding Mechanism of Enzyme–Photosensitizer Facilitates Catalysis-Augmented Photodynamic Therapy, *Research*, 2025, **8**, 0732, DOI: 10.34133/research.0732.

16 V. Aggarwal, D. Singh, A. Hooda, K. Jakhar, S. Kumar, R. S. Malik and P. Kumar, Optimizing europium(III) ion luminescence *via* β-diketone and auxiliary ligands: analysis of optoelectronic features and Judd-Ofelt parameters, *Chem. Phys. Lett.*, 2025, 142244, DOI: 10.1016/j.cplett.2025.142244.

17 C. Q. Shen, T. L. Yan, Y. T. Wang, Z. J. Ye, C. J. Xu and W. J. Zhou, Synthesis, structure and luminescence properties of binary and ternary complexes of lanthanide (Eu^{3+}, Sm^{3+} and Tb(III)) with salicylic acid and 1,10-phenanthroline, *J. Lumin.*, 2017, **184**, 48–54, DOI: 10.1016/j.jlumin.2016.12.018.

18 S. A. Ansari, L. Liu and L. Rao, Binary lanthanide(III)/nitrate and ternary lanthanide(III)/nitrate/chloride complexes in an ionic liquid containing water: optical absorption and luminescence studies, *Dalton Trans.*, 2015, **44**, 2907–2914, DOI: 10.1039/C4DT03479A.

19 V. Aggarwal, D. Singh, S. Bhagwan, R. K. Saini, K. Jakhar, R. S. Malik, P. Kumar and J. Sindhu, Exploring the influence of emissive centers in mono and dinuclear europium(III) complexes for advance lighting applications: Synthesis, characterization and computational modeling, *J. Mol. Struct.*, 2025, **1324**, 140841, DOI: 10.1016/j.molstruc.2024.140841.

20 K. Nehra, A. Dalal, A. Hooda, D. Singh, S. Kumar and R. S. Malik, Heteroleptic luminous ternary europium Complexes: Synthesis, electrochemical and photophysical investigation, *Chem. Phys. Lett.*, 2022, **800**, 139675, DOI: 10.1016/j.cplett.2022.139675.

21 Q. Zhou, F. Yang, D. Liu, Y. Peng, G. Li, Z. Shi and S. Feng, Synthesis, structures, and magnetic properties of three fluoride-bridged lanthanide compounds: effect of bridging fluoride ions on magnetic behaviors, *Inorg. Chem.*, 2012, **51**, 7529–7536, DOI: 10.1021/ic300125y.

22 W. K. Wong, X. Zhu and W. Y. Wong, Synthesis, structure, reactivity and photoluminescence of lanthanide(III) monoporphyrinate complexes, *Coord. Chem. Rev.*, 2007, **251**, 2386–2399, DOI: 10.1016/j.ccr.2006.11.014.

23 G. Li, D. Zhu, X. Wang, Z. Su and M. R. Bryce, Dinuclear metal complexes: multifunctional properties and applications, *Chem. Soc. Rev.*, 2020, **49**, 765–838, DOI: 10.1039/C8CS00660A.

24 A. Dalal, K. Nehra, A. Hooda, D. Singh, J. Dhankhar and S. Kumar, Fluorinated β-diketone-based Sm(III) complexes: spectroscopic and optoelectronic characteristics, *Luminescence*, 2022, **37**, 1328–1334, DOI: 10.1002/bio.4300.

25 Y. Wang, X. Meng, W. Shi, Y. Xie, A. Liu, L. Xu, L. Qiu, X. Song, M. Zhang, J. Zhang and J. Yu, Single-atom Cu anchored on a UiO-66 surface-enhanced Raman scattering sensor for trace and rapid detection of volatile organic compounds, *Research*, 2025, **8**, 0841, DOI: 10.34133/research.0841.

26 D. Nguyen Thi, N. Nguyen Thi, A. T. Vu, T. Q. Tran, T. Nguyen Ngoc, D. Luong Xuan, T. Ta Thi and T. Nguyen Xuan, Pyridinedicarboxylate-Tb(III) Complex-Based Luminescent Probes for ATP Monitoring, *J. Anal. Methods Chem.*, 2021, **2021**, 7030158, DOI: 10.1155/2021/7030158..

27 V. Aggarwal, D. Singh, S. Bhagwan, R. K. Saini, K. Jakhar, S. Kumar, P. Kumar and J. Sindhu, Tuning emissive color of trivalent terbium ion through environmental factors: optoelectronic insights from theoretical, spectral and computational studies, *RSC Adv.*, 2024, **14**, 3956939587, DOI: 10.1039/D4RA05334F.

28 M. A. Girsova, G. F. Golovina, I. N. Anfimova and L. N. Kurilenko, Infrared spectroscopy study of silver-containing composite materials based on nanoporous silicate glass doped with Tb(III) or Sm^{3+} ions, *Glass Phys. Chem.*, 2019, **45**, 325–331, DOI: 10.1134/S1087659619050055.

29 G. Qian-Ling, Z. Wen-Xiang, G. Rong, Y. Xi and W. Ru-Ji, Crystal Structure of Complex Tris (4,4,4-trifluoro-1-pheny1–1,3-butanedione)(1,10-phenanthroline) Europium(III), *Chin. J. Chem.*, 2003, **21**, 211–215, DOI: 10.1002/cjoc.20030210225.

30 V. Aggarwal, D. Singh, S. Redhu, S. Malik, S. Dalal, S. Kumar, R. S. Malik, P. Kumar and J. Sindhu, Design and photophysical characterization of dinuclear lanthanide complexes incorporating spacer ligands along with their mononuclear analogues: A comparative study, *Opt. Mater.*, 2024, **155**, 115833, DOI: 10.1016/j.optmat.2024.115833.

31 A. Hooda, D. Singh, A. Dalal, K. Nehra, S. Kumar, R. S. Malik, H. Sehrawat and P. Kumar, N-donor auxiliary ligand-based terbium(III) β-diketonates: Preparation and photophysical studies, *J. Lumin.*, 2023, **258**, 119828, DOI: 10.1016/j.jlumin.2023.119828.

32 C. F. Liang, E. J. Schmitschek and J. A. Trias, *J. Inorg. Nucl. Chem.*, 1970, **32**, 811–831.

33 K. Iftikhar, A. U. Malik and N. Ahmad, *J. Chem. Soc., Dalton Trans.*, 1985, 2547–2550, DOI: 10.1039/dt9850002547.

34 V. Aggarwal, D. Singh, S. Redhu, S. Bhagwan, S. Kumar, R. S. Malik, P. Kumar, J. Sindhu and V. Kumar, Pyrazine-driven dinuclear assembly of dysprosium(iii) β-diketonate complex: a fluxidentate bridging approach toward functional near-white luminescent materials, *RSC Adv.*, 2025, **15**, 49227–49242, DOI: 10.1039/D5RA05762K.

35 V. Aggarwal, D. Singh, K. Nehra, S. Dalal, S. Redhu, P. Kumar, S. Kumar and R. S. Malik, White light emission from a ternary dysprosium complex: Energy transfer and ligand-driven modulation, *Mater. Sci. Semicond. Process.*, 2025, **192**, 109427, DOI: 10.1016/j.mssp.2025.109427.

36 A. Ali, Z. Ahmed and K. Iftikhar, Heteroleptic samarium complexes with high quantum yields for temperature sensing applications, *Dalton Trans.*, 2024, **53**, 1105–1120, DOI: 10.1039/D3DT03160H.

37 V. Aggarwal, D. Singh, P. Kumar, S. Dalal, S. Kumar, R. S. Malik, P. Kumar, J. Sindhu and H. Kumar, DFT Studies and Experimental Characterization of Eu^{3+} Complexes in Different Coordinating Environment: A Comprehensive Approach to Luminescence and Applications in Display Technologies, *J. Mol. Struct.*, 2025, 142781, DOI: 10.1016/j.molstruc.2025.142781.

38 B. Klein and J. Berkowitz, Pyrazines. I. Pyrazine-N-oxides. Preparation and Spectral Characteristics, *J. Am. Chem. Soc.*, 1959, **81**, 5160–5166, DOI: 10.1021/ja01528a035.

39 V. Aggarwal, D. Singh, A. Hooda, K. Nehra, S. Redhu, S. Kumar, R. S. Malik and P. Kumar, Design and spectroscopic study of samarium complexes with tunable photoluminescent properties, *J. Mol. Struct.*, 2024, **1311**, 138315, DOI: 10.1016/j.molstruc.2024.138315.

40 A. Dolgonos, T. O. Mason and K. R. Poeppelmeier, Direct optical band gap measurement in polycrystalline semiconductors: A critical look at the Tauc method, *J. Solid State Chem.*, 2016, **240**, 43–48, DOI: 10.1016/j.jssc.2016.05.010.

41 A. Hooda, K. Nehra, A. Dalal, S. Singh, S. Bhagwan, K. Jakhar and D. Singh, Preparation and photoluminescent analysis of Sm^{3+} complexes based on unsymmetrical conjugated chromophoric ligand, *J. Mater. Sci.: Mater. Electron.*, 2022, **33**, 11132–11142, DOI: 10.1007/s10854-022-08089-w.

42 E. Berti, A. Caneschi, C. Daiguebonne, P. Dapporto, M. Formica, V. Fusi, L. Giorgi, A. Guerri, M. Micheloni, P. Paoli and R. Pontellini, Ni(II), Cu(II), and Zn(II) Dinuclear Metal Complexes with an Aza−Phenolic Ligand: Crystal Structures, Magnetic Properties, and Solution Studies, *Inorg. Chem.*, 2003, **42**, 348–357, DOI: 10.1021/ic0204070.

43 A. Dalal, K. Nehra, A. Hooda, S. Singh, D. Singh and S. Kumar, Synthesis, optoelectronic and photoluminescent characterizations of green luminous heteroleptic ternary terbium complexes, *J. Fluoresc.*, 2022, **32**, 1019–1029, DOI: 10.1007/s10895-022-02920-7.

44 A. N. Neto, E. Kasprzycka, A. S. Souza, P. Gawryszewska, M. Suta, L. D. Carlos and O. L. Malta, On the long decay time of the $^7F_5$ level of Tb(III), *J. Lumin.*, 2022, **248**, 118933, DOI: 10.1016/j.jlumin.2022.118933.

45 S. Dalal, D. Singh, A. Dalal, A. Hooda, S. Kumar, R. S. Malik, P. Kumar and J. Sindhu, Green emissive Tb(III) complexes based on photosensitizing antenna: Synthesis and optoelectronic analysis, *Mater. Sci. Semicond. Process.*, 2024, **177**, 108370, DOI: 10.1016/j.mssp.2024.108370.

46 K. Nehra, A. Dalal, A. Hooda, S. Singh and D. Singh, Computational and spectroscopic evaluation of 1,10-phenanthroline based Eu(III) fluorinated β-diketonate complexes for displays, *J. Lumin.*, 2022, **251**, 119111, DOI: 10.1016/j.jlumin.2022.119111.

47 V. Aggarwal, D. Singh, A. Hooda, K. Nehra, K. Jakhar, S. Kumar, R. S. Malik and P. Kumar, Synthesis and photoluminescent analyses of ternary terbium(III) Tris-β-

diketonate complexes: A systematic exploration, *J. Mater. Sci.: Mater. Electron.*, 2024, **35**, 568, DOI: 10.1007/s10854-024-12314-z.

48 R. T. Moura Jr, A. N. Neto, R. L. Longo and O. L. Malta, On the calculation and interpretation of covalency in the intensity parameters of 4f–4f transitions in Eu^{3+} complexes based on the chemical bond overlap polarizability, *J. Lumin.*, 2016, **170**, 420–430, DOI: 10.1016/j.jlumin.2015.08.016.

49 W. M. Wang, H. X. Zhang, S. Y. Wang, H. Y. Shen, H. L. Gao, J. Z. Cui and B. Zhao, Ligand field affected Single-Molecule Magnet behavior of lanthanide(III) dinuclear complexes with an 8-hydroxyquinoline Schiff base derivative as bridging ligand, *Inorg. Chem.*, 2015, **54**, 10610–10622, DOI: 10.1021/acs.inorgchem.5b01404.

50 V. Aggarwal, D. Singh, P. Kumar, A. Hooda, S. Malik, J. Sindhu, P. Kumar, S. Kumar and R. S. Malik, Synthesis and Characterization of Near-White Luminescent Tb(III) β-Diketonates for Potential OLED Applications: Influence of Neutral co-ligands on Optical and Electronic Properties, *J. Mol. Struct.*, 2025, 145049, DOI: 10.1016/j.molstruc.2025.145049.

51 A. Dalal, K. Nehra, A. Hooda, D. Singh, S. Kumar and R. S. Malik, Red emissive ternary europium complexes: synthesis, optical, and luminescence characteristics, *Luminescence*, 2022, **37**, 1309–1320, DOI: 10.1002/bio.4297.

52 W. A. Dar, Z. Ahmed and K. Iftikhar, Cool white light emission from the yellow and blue emission bands of the Dy(III) complex under UV-excitation, *J. Photochem. Photobiol., A*, 2018, **356**, 502–511, DOI: 10.1016/j.jphotochem.2017.12.017.

53 Z. Ahmed and K. Iftikhar, Efficient layers of emitting ternary lanthanide complexes for fabricating red, green, and yellow OLEDs, *Inorg. Chem.*, 2015, **54**, 11209–11225, DOI: 10.1021/acs.inorgchem.5b01630.

54 S. V. Eliseeva, O. V. Kotova, F. Gumy, S. N. Semenov, V. G. Kessler, L. S. Lepnev, J. C. Bünzli and N. P. Kuzmina, Role of the ancillary ligand *N*,*N*-dimethylaminoethanol in the sensitization of EuIII and TbIII luminescence in dimeric β-diketonates, *J. Phys. Chem. A*, 2008, **112**, 3614–3626, DOI: 10.1021/jp711305u.

55 A. P. Samuel, E. G. Moore, M. Melchior, J. Xu and K. N. Raymond, Water-soluble 2-hydroxyisophthalamides for sensitization of lanthanide luminescence, *Inorg. Chem.*, 2008, **47**, 7535–7544, DOI: 10.1021/ic800328g.

56 R. Ilmi and K. Iftikhar, Optical emission studies of new europium and terbium dinuclear complexes with trifluoroacetylacetone and bridging bipyrimidine. Fast radiation and high emission quantum yield, *Polyhedron*, 2015, **102**, 16–26, DOI: 10.1016/j.poly.2015.07.046.

57 K. Burek, S. Eidner, S. Kuke and M. U. Kumke, Intramolecular deactivation processes of electronically excited lanthanide(III) complexes with organic acids of low molecular weight, *Spectrochim. Acta, Part A*, 2018, **191**, 36–49, DOI: 10.1016/j.saa.2017.09.012.

58 B. Yan and B. Zhou, Photophysical properties of dysprosium complexes with aromatic carboxylic acids by molecular spectroscopy, *J. Photochem. Photobiol., A*, 2005, **171**, 181–186, DOI: 10.1016/j.jphotochem.2004.10.012.

59 V. Misra and H. Mishra, Photoinduced proton transfer coupled with energy transfer: Mechanism of sensitized luminescence of terbium ion by salicylic acid doped in polymer, *J. Chem. Phys.*, 2008, **128**(24), 244701, DOI: 10.1063/1.2918284.

60 X. Zhang, Y. Wang, X. Wu, F. Wang, Q. Ou and S. Zhang, A Comprehensive Review on Mechanisms and Applications of Rare-Earth Based Perovskite Nanocrystals, *Chin. J. Chem.*, 2024, **42**, 1032–1056, DOI: 10.1002/cjoc.202300344.

61 Z. Yonghui, C. Mindong, G. U. Shengli, X. U. Jianqiang, G. Guizhi, K. O. Qinggang, H. Gang, L. Jun, M. A. Yan, G. U. Yan and Y. Zheng, Photoluminescence properties of dinuclear lanthanide complexes in visible and near-infrared region, *J. Rare Earths*, 2010, **28**, 660–665, DOI: 10.1016/S1002-0721(09)60174-5.

62 D. Singh, R. K. Saini and S. Bhagwan, Recent developments in dye-sensitized solar cells and potential applications, *Emerging Photovoltaic Materials: Silicon & Beyond*, 2018, pp. 443–486, DOI: 10.1002/9781119407690.

63 C. W. Jin, Q. Q. Zhao, N. Ren, J. J. Zhang, L. N. Geng, S. P. Wang and S. K. Shi, Preparation, Crystal Structures and Properties of a Series of Novel Lanthanide Complexes Based on 2,3-Dimethoxybenzoic Acid and 1,10-Phenanthroline, *Polyhedron*, 2017, **135**, 206–215, DOI: 10.1016/j.poly.2017.06.050.

64 E. R. Dos Santos, R. O. Freire, N. B. Da Costa, F. A. A. Paz, C. A. De Simone, S. A. Júnior, A. A. S. Araújo, L. A. O. Nunes, M. E. De Mesquita and M. O. Rodrigues, Theoretical and Experimental Spectroscopic Approach of Fluorinated Ln^{3+}-b-Diketonate Complexes, *J. Phys. Chem. A*, 2010, **114**, 7928–7936, DOI: 10.1021/jp104038r.

65 N. Hasan and K. Iftikhar, Syntheses, Crystal Structure and Photophysical Properties of $[Sm(Dbm)_3(Impy)]$ and $[Tb(Dbm)_3(Impy)]$ and Their Hybrid Films, *New J. Chem.*, 2019, **43**, 4391–4405, DOI: 10.1039/c8nj05045g.

66 A. B. Ganaie, A. Ali and K. Iftikhar, Synthesis, Structure, Phase Controlled Colour Tuning of Dinuclear Pr(III) and Tb(III) Complexes with Fluorinated b-Diketone and Heterocyclic Lewis Base as UV Light Converters, *Polyhedron*, 2022, **212**, 115592, DOI: 10.1016/j.poly.2021.115592.

67 F. A. Silva, H. A. Nascimento, D. K. S. Pereira, E. E. S. Teotonio, H. F. Brito, M. C. F. C. Felinto, J. G. P. Espínola, G. F. Sa and W. M. Faustino, Energy Transfer Processes in Tb(III)-Dibenzoylmethanate Complexes with Phosphine Oxide Ligands, *J. Braz. Chem. Soc.*, 2013, **24**, 601–608, DOI: 10.5935/0103-5053.20130073.

68 T. Zahariev, D. Shandurkov, S. Gutzov, N. Trendafilova, D. Enseling, T. Jüstel and I. Georgieva, Phenanthroline chromophore as efficient antenna for Tb(III) green luminescence: A theoretical study, *Dye Pigm.*, 2021, **185**, 108890, DOI: 10.1016/j.dyepig.2020.108890.

69 W. A. Dar and K. Iftikhar, Phase controlled colour tuning of samarium and europium complexes and excellent photostability of their PVA encapsulated materials, Structural

elucidation, photophysical parameters and the energy transfer mechanism in the Eu^{3+} complex by Sparkle/PM3 calculations, *Dalton Trans.*, 2016, **45**, 8956–8971, DOI: 10.1039/C6DT00549G.

70 M. J. Beltrán-Leiva, D. Páez-Hernández and R. Arratia-Pérez, Theoretical determination of energy transfer processes and influence of symmetry in Lanthanide(III) complexes: Methodological considerations, *Inorg. Chem.*, 2018, **57**, 5120–5132, DOI: 10.1021/acs.inorgchem.8b00159.

71 E. M. Chan, Combinatorial approaches for developing upconverting nanomaterials: high-throughput screening, modeling, and applications, *Chem. Soc. Rev.*, 2015, **44**, 1653–1679, DOI: 10.1039/C4CS00205A.

72 W. T. Carnall, P. R. Fields and K. Rajnak, *J. Chem. Phys.*, 1968, **1968**, 49.

73 P. Kumari, V. Lather, P. Ahlawat, M. Kumar and R. Kumar, Lasing properties, Judd-Ofelt and band gap investigation of cool green emanating Tb(III) complexes for solid and solution state luminescence, *Opt. Mater.*, 2024, **147**, 114677, DOI: 10.1016/j.optmat.2023.114677.

74 W. T. Carnall, P. R. Fields and K. Rajnak, Spectral intensities of the trivalent lanthanides and actinides in solution. II. Pm^{3+}, Sm^{3+}, Eu^{3+}, Gd^{3+}, Tb(III), Dy^{3+}, and Ho^{3+}, *J. Chem. Phys.*, 1968, **49**, 4412–4423, DOI: 10.1063/1.1669892.

75 J. H. Monteiro, I. O. Mazali and F. A. Sigoli, Determination of Judd-Ofelt intensity parameters of pure samarium(III) complexes, *J. Fluoresc.*, 2011, **21**, 2237–2243, DOI: 10.1007/s10895-011-0928-x.

76 B. C. Jamalaiah, J. S. Kumar, A. M. Babu, T. Suhasini and L. R. Moorthy, Photoluminescence properties of Sm^{3+} in LBTAF glasses, *J. Lumin.*, 2009, **129**, 363–369, DOI: 10.1016/j.jlumin.2008.11.001.

77 A. Aebischer, F. Gumy and J. C. Bünzli, Intrinsic quantum yields and radiative lifetimes of lanthanide tris (dipicolinates), *Phys. Chem. Chem. Phys.*, 2009, **11**, 1346–1353, DOI: 10.1039/B816131C.

78 M. D. Hanwell, D. E. Curtis, D. C. Lonie, T. Vandermeerschd, E. Zurek and G. R. Hutchison, Avogadro: An advanced semantic chemical editor, visualization, and analysis platform, *J. Cheminf.*, 2012, **4**, 1, DOI: 10.1186/1758-2946-4-17.

79 F. Weigend and R. Ahlrichs, Balanced basis sets of split valence, triple zeta valence and quadruple zeta valence quality for H to Rn: Design and assessment of accuracy, *Phys. Chem. Chem. Phys.*, 2005, **7**, 3297–3305, DOI: 10.1039/B508541A.

80 M. Dolg, H. Stoll, A. Savin and H. Preuss, Energy-adjusted pseudopotentials for the rare earth elements, *Theor. Chim. Acta*, 1989, **75**, 173–194, DOI: 10.1007/BF00528565.

81 M. Dolg, H. Stoll and H. Preuss, Energy-adjusted ab initio pseudopotentials for the rare earth elements, *J. Chem. Phys.*, 1989, **90**, 1730–1734, DOI: 10.1063/1.456066.

82 X. Cao, M. Dolg and H. Stoll, Valence basis sets for relativistic energy-consistent small-core actinide pseudopotentials, *J. Chem. Phys.*, 2003, **118**, 487–496, DOI: 10.1063/1.1406535.

83 F. Neese, The ORCA program system, *Rev.: Comput. Mol. Sci.*, 2012, **2**, 73, DOI: 10.1002/wcms.81.

84 T. Koopmans, Über die Zuordnung von Wellenfunktionen and Eigenwertenzu den EinzelnenElektronenEines Atoms, *Physica*, 1934, **1**, 104–113, DOI: 10.1016/S0031-8914(34)90011-2.

85 R. Vijayaraj, V. Subramanian and P. K. Chattaraj, Comparison of global reactivity descriptors calculated using various density functionals: a QSAR perspective, *J. Chem. Theory Comput.*, 2009, **5**, 2744, DOI: 10.1021/ct900347f.